BUTTERWORTH HEINEMANN

Polymer Vol. 36 No. 20, pp. 3863–3873, 1995

0032-3861/95/$10.00+0.00

Drawing and annealing of nylon-6 fibres: studies of crystal growth, orientation of amorphous and crystalline domains and their influence on properties

N. S. Murthy* and R. G. Bray
Research and Technology, AlliedSignal Inc., PO Box 1021, Morristown, NJ 07962, USA

and S. T. Correale and R. A. F. Moore
Fibers Division, AlliedSignal Inc., PO Box 31, Petersburg, VA 23804, USA
(Received 13 March 1995; revised 4 May 1995)

Structural changes in nylon-6 fibres that occur during processing are analysed using X-ray diffraction (X.r.d.), optical birefringence, density and infra-red (i.r.) spectroscopy methods. Amorphous orientation is described completely by a single parameter, degree of orientation, on the basis of i.r. and optical birefringence measurements. But an additional parameter, the fraction of oriented or anisotropic amorphous component, was necessary to fully interpret the X.r.d. data. The amorphous orientation increases as expected upon drawing, but decreases upon annealing at all temperatures. Crystalline orientation increases rapidly at small draw ratios (<3) and reaches a plateau at higher draw ratios. Crystalline orientation decreases upon annealing in highly drawn fibres but increases in others. The crystallinity is ~15% in the undrawn fibre, and continues to increase beyond the ~ 50% value measured for the fibre with the highest (4.5×) draw ratios used here. Secondary crystallization during drawing occurs at the expense of unoriented amorphous fraction, and in the initial stages of drawing (3×) is accompanied by the transformation of the γ into the α crystalline form. Secondary crystallization during annealing occurs at the expense of the oriented amorphous fraction. The ease of γ to α conversion during annealing depends on the initial state of the γ form. The glass transition temperature (T_g) appears to be determined solely by the amorphous orientation, being higher in fibres with a higher anisotropic component. The improved mechanical properties observed at higher draw ratios are attributed to higher crystallinity and lower fraction of the unoriented amorphous component. The shrinkage observed upon annealing of fibres with smaller draw ratios (~3) is likely to be the result of the crystallization of the oriented amorphous chain segments.

(Keywords: nylon-6 fibres; mechanical properties; crystallization)

INTRODUCTION

Among the many morphological characteristics of a fibre, crystallinity, degree of crystalline perfection, lamellar spacings and orientations of the crystalline and amorphous regions are probably the most frequently used parameters for predicting the performance of a fibre. Changes in some of these parameters are very likely correlated with each other[1,2]. Once the limiting crystallinity of a fibre is reached, typically 75% in polyethylene, 55% in nylon-6,6, 50% in nylon-6 and 35% in poly(ethylene terephthalate), further enhancement in properties such as tenacity, modulus, shrinkage and dyeability is usually achieved by increasing the orientation of the crystallites and the amorphous chain segments[3,4]. We use the term 'amorphous' to describe all of the non-crystalline domains. The crystalline orientation has been traditionally measured to a high accuracy and precision by X-ray diffraction (X.r.d.)[5], but a reliable measurement of amorphous orientation has remained elusive[6–8], particularly in commercially important fibres with trilobal cross-section. We have therefore begun a programme to characterize the amorphous phase in semicrystalline polymers[4,7,8]. Here we investigate the influence of drawing and heat setting on the amorphous phase in nylon-6, and determine the accompanying changes in the crystallinity and phase composition using X.r.d., infra-red spectroscopy (i.r.), optical birefringence and density measurements. The significance of these results is illustrated by correlating the structural changes to glass transition temperature and shrinkage behaviour of nylon fibres.

EXPERIMENTAL

Materials

Two series of yarns were studied. In one series, commercial nylon-6 yarns (labelled A, B, C and D), with varying degree of α and γ crystalline fractions, were analysed to study the effect of heat setting in an autoclave at 270°F (~ 132°C). In the second series,

* To whom correspondence should be addressed

undrawn and drawn (2.5, 3, 3.5, 4 and 4.5×) round cross-section fibres were used to investigate the effect of draw ratio (*DR*).

X-ray diffraction

X.r.d. scans were obtained on a Philips diffractometer in the transmission mode using Cu Kα radiation with a graphite monochromator in the diffracted beam. The yarn was wound on a comb-like sample holder so as to maintain the individual filaments parallel to each other. The scans were typically collected between $2\theta = 6°$ and 35°. Radial scans with the sample spinning at 60 rev min^{-1} in its own plane and perpendicular to the beam (fast-rotational scan) were obtained to determine the crystallinity. Equatorial scans were obtained to determine the phase composition and the crystallite sizes. A sequence of radial scans (25–30) at a series of azimuthal angles ϕ (−90° to 90°, equator being 0°) were obtained by rotating the sample by 5–10° between successive radial scans.

The radial scans between $2\theta = 6°$ and 29° obtained at various azimuthal angles were resolved into crystalline (α and γ) and amorphous peaks using a non-linear least-squares procedure. Pearson VII functions were used in these analyses, and the shape factor was ~2 for most fits. The various peaks and their typical 2θ and ϕ values are given in *Table 1*. The scans ca. 20° on either side of the equator (E scans) were fitted to an amorphous halo, and two α (α_1 and α_2) and two γ (γ_1 and γ_2) crystalline peaks. Scans ca. 20° on either side of the meridian (M scans) were fitted to the (0 2 0) γ crystalline peak, a (0 4 0) $\alpha + \gamma$ crystalline peak, and an amorphous halo. Peaks corresponding to layer lines (subscript L in *Table 1*) were included in the analysis of scans within a ca. 50° sector between the equator and the meridional axes (R scans). Some of the peaks in the R scans also appear in the E or M scans. The parameters of these peaks were constrained during the fitting of the R scans on the basis of the analyses of E and M scans. Such constraints were found to be necessary to reduce the number of independent parameters and thus obtain meaningful results. The heights of the amorphous and crystalline peaks were plotted as a function of azimuthal angle. This plot is used to calculate two characteristics of the amorphous phase related to orientation as described under the 'Results' section.

Infra-red spectroscopy

Polarized i.r. spectra were measured on a Mattson Cygnus 100 FT-IR spectrometer at a resolution of 4 cm^{-1} using both macro- and microsampling techniques. Macrosampling (using a photoacoustic detector, MTEC-200) averages the effects of the fibre twists and kinks, and the resulting i.r. spectra are of poorer quality than can be obtained by microsampling techniques (Spectra-Tech IR-Plan), especially for polarization studies. Measurements using the i.r. microscope in transmission mode yielded superior spectra with much higher signal-to-noise ratio and shorter acquisition times. Apart from the lower signal-to-noise ratio, the spectra were essentially the same as for the macrosampling despite the potential problems associated with sampling microscopic areas of the fibres such as lobes in trilobal fibres. Hence, only the data from the microsampling technique are reported here.

Specific i.r. bands (1000–880 cm^{-1}) characteristic of the α, γ and amorphous phases were resolved using a non-linear, least-squares curve resolution program to determine the orientation and relative changes in composition of each phase. The peaks were assumed to be Lorentzian with a linear baseline. Generally, constraints were imposed on the fitted parameters to obtain consistent and reliable results. For the α phase, the parameters for best fit were determined on the prominent peaks of the high-draw-ratio polarized spectra. The widths were then held constant when the peak intensity was very low. The bands for the amorphous and the γ phases overlap considerably with each other and with one of the α phase bands. Both width and frequency constraints were determined from spectra where these bands were prominent and then imposed on the remaining spectra. While this reduces the accuracy in the determination of orientation and composition, especially for the amorphous and γ phases relative to α, it does not interfere with our ability to discern trends in phase content and orientation with processing conditions.

Density, birefringence and glass transition temperature

Density was measured using a density gradient column with carbon tetrachloride/heptane solution (1.3–1.16 g cm^{-3}) at 23°C. Birefringence was measured on a Leitz polarizing microscope using a Berek compensator. The birefringence data were used to determine the amorphous orientation, f_{ab}, according to the expression[6]:

$$\Delta = f_{ab}(1 - x_c)\Delta_a + f_c x_c \Delta_c \qquad (1)$$

in which Δ is the measured optical birefringence, x_c is the crystallinity, f_c is the crystalline orientation, and Δ_a and Δ_c are the intrinsic optical birefringences of the amorphous and the crystalline domains, respectively. The value of f_{ab} was determined using $\Delta_a = 0.078$ and $\Delta_c = 0.089$ (ref. 9).

T_g measurements were carried out on fibres stored under ambient conditions (23°C and ~45% relative humidity) using a Sieko oscillatory d.s.c. instrument. A 10°C amplitude at 0.01 Hz from −30 to 300°C at a heating rate of 10°C min^{-1} was used.

Table 1 X-ray peak positions

Peak identification	Azimuthal angle, ϕ (deg)	Radial angle, 2θ (deg)
α_1	0	20.0
α_2	0	24.0
γ_1	0	21.5
γ_2	0	23.0
α_M	90	21.0
γ_M	90	10.5
α_{L1}	26	21.5
α_{L2}	45	14.5
α_{L3}	66	27.2
γ_{L1}	15	19.0
γ_{L2}	27	24.5
amorph.	90–0	20.0–22.0

RESULTS AND ANALYSIS

X-ray diffraction

Schematic X.r.d. photographs of α- and γ-rich nylon-6

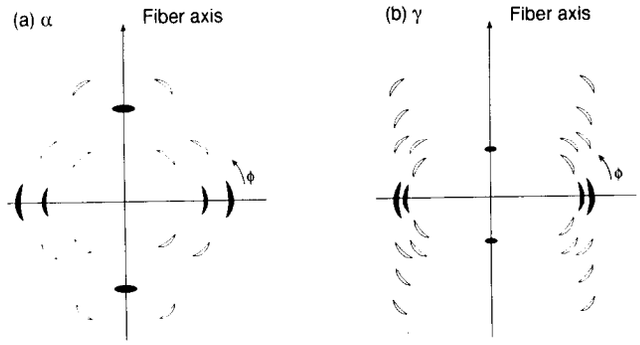

Figure 1 Schematic of the X-ray diffraction pattern from oriented nylon-6 fibres in which the crystalline form is (a) α from fibre D(HS) (see *Table 2*), and (b) γ from the 4.5× drawn fibre after iodine treatment

fibres are shown in *Figure 1*. Radial diffraction scans obtained at various azimuthal angles from these two types of fibres are shown in *Figure 2*. We initially attempted to calculate the crystallinity from fast rotational scans using all the peaks given in *Table 1*. But, to simplify the procedure and to obtain reproducible values, profile analysis of the type shown in *Figure 3*, using only one layer line reflection at $2\theta \sim 14°$, was used. A crystalline index (CI) useful for internal comparison within the set of fibres in this study was calculated from the ratio of the four equatorial crystalline peaks (α_1, α_2, γ_1 and γ_2; see *Table 1*) to the total scattering area; the peaks at 11° (meridional, *Table 1*) and 14° (layer line) were not included in the crystallinity calculations. An example of the profile analysis of a radial scan fitted according to the method described under 'Experimental' is shown in *Figure 4*.

Profile analysis of the equatorial scans was used to obtain the α/γ ratio from the areas of the corresponding peaks. The equatorial scans were also used to obtain an apparent crystallite size (ACS)[10] and an index of crystalline perfection (ICP)[2] from the expressions:

$$ACS = 0.9\lambda/(\Delta\theta \cos\theta) \tag{2}$$

$$ICP = 2\theta(\alpha_2) - 2\theta(\alpha_1) \tag{3}$$

in which λ is the wavelength (1.542 Å), 2θ is the peak position, $\Delta\theta$ is the full-width at half-maximum in the radial direction, and α_1 and α_2 are, respectively, the (200) and (002+202) crystalline peaks of the α crystalline form.

The intensities of the amorphous and the crystalline peaks were plotted as a function of the azimuthal angle (ϕ) to quantify the orientation in the crystalline and the amorphous domains (*Figure 5*). Unlike in a simple azimuthal scan at a fixed 2θ, these scans plot the intensity maxima obtained from the analysis of the type shown in *Figure 4*, and hence they may not represent the intensity at a fixed 2θ. This is especially true for the amorphous halo whose maximum shifts to lower 2θ angles in going from the equator to the meridian. The azimuthal intensity distribution of the crystalline peaks, $I_c(\phi)$, could be defined by a single parameter, the full-width at half-maximum ($\Delta\phi$) of the peak. The degree of crystalline orientation (f_c) was calculated from this width using the expression[5]:

$$f_c = (3\langle\cos^2\phi\rangle - 1)/2 \tag{4}$$

$$\langle\cos^2\phi\rangle = \int_{-\pi/2}^{\pi/2} I_c(\phi)\cos^2\phi \sin\phi \, d\phi \Big/ \int_{-\pi/2}^{\pi/2} I_c(\phi)\sin\phi \, d\phi \tag{5}$$

$$I_c(\phi) = \exp[-\ln 2(2\phi/\Delta\phi)^2] \tag{6}$$

Unlike the crystalline peaks in even the least-oriented undrawn fibres, the amorphous peaks in even the most-oriented highly drawn fibres have a non-zero baseline. The integrated intensity under the baseline is a significant fraction of the total amorphous scattering. Thus, whereas the crystalline azimuthal scans could be completely described by the width of the peak, an additional parameter is necessary to account for this baseline scattering in amorphous azimuthal plots. To analyse such data, the intensity is separated into two components, the isotropic component under the baseline and the anisotropic component above the baseline. The isotropic scattering is attributed to the randomly oriented amorphous chain segments. The Gaussian component above the baseline is attributed to the scattering from the anisotropic component of the

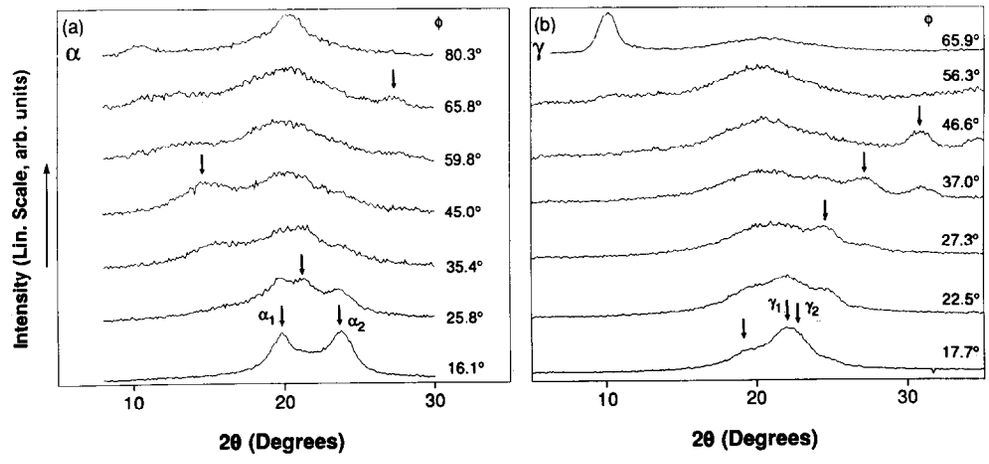

Figure 2 A sequence of radial scans at a series of azimuthal angles from fibres in which the crystalline form is either (a) primarily α or (b) primarily γ. The scans have been scaled separately so that the intensity maximum in each of the scans is of about the same height. Thus the intensity scales for the various scans are not the same. The various peaks are listed in *Table 1*

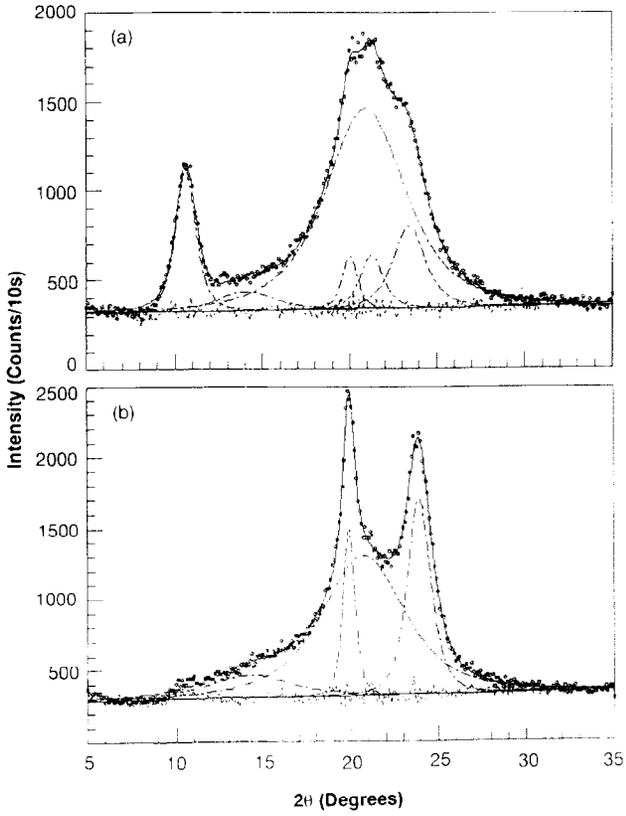

Figure 3 Profile analysis of the fast rotational scan for crystallinity determinations. The scans (a) and (b) are from fibre C (*Table 3*) before and after annealing, respectively. In this figure and *Figure 4*, the filled circles are observed intensitites, the broken lines are the resolved components, the full line through the circles is the sum of the resolved components, the base line is shown by the lower full line, and the dotted line near the base line is the difference between the observed and fitted intensities

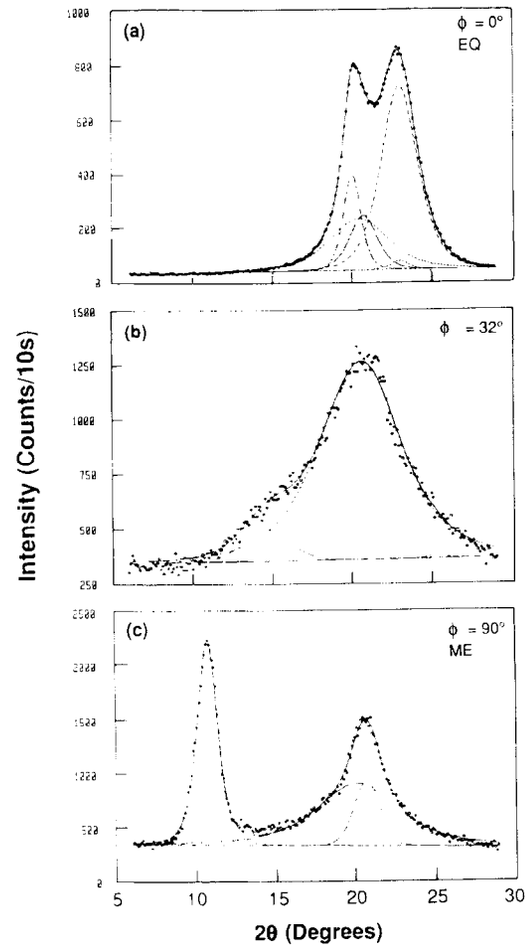

Figure 4 Details of profile analysis at three azimuthal angles. (a) An equatorial scan ($\phi = 0°$) resolved into two α reflections (α_1 at ~21° and α_2 at ~24°) and two γ reflections (γ_1 at ~22° and γ_2 at ~23°) and an amorphous halo. (b) An off-axis scan ($\phi = 32°$ from the equator) resolved into a layer line reflection and an amorphous halo. (c) A meridional reflection ($\phi = 90°$) resolved into a γ_{020} reflection at 11°, a $(\alpha + \gamma)_{040}$ reflection at 21° and an amorphous halo

amorphous phase, i.e. amorphous chain segments oriented preferentially along the fibre axis.

To quantify the amorphous anisotropy, we will define a term F_{oa} as the fraction of the molecules in the amorphous regions that are preferentially oriented. This fraction of the anisotropic or oriented amorphous component can be calculated as:

$$F_{oa} = A_p/(A_p + A_b) \tag{7}$$

where A_p is the area of the amorphous peak above the baseline and A_b is the intensity below the baseline, $(A_p + A_b)$ being the total scattered intensity from the amorphous phase. We will quantify the degree of orientation of this oriented fraction by the term f_{oa}, which can be calculated from the width $\Delta\phi$ of the amorphous peak above the baseline using equation (4) by replacing I_c in equations (5) and (6) with I_{oa}, the intensity from the oriented amorphous phase. In equation (6) $\Delta\phi$ is the full-width at half-maximum of the amorphous peak above the baseline. Lastly, we can calculate an average degree of amorphous orientation for the entire amorphous phase on the basis of the X-ray data (f_{ax}) from the total azimuthal intensity distribution of the amorphous halo using equation (4) by replacing I_c in equation (5) with I_{ax}, the intensity of the total amorphous scattering. Since f_{ax} is determined using the entire amorphous X-ray scattering, this term can be used to compare with parameters such as f_{ab} (equation (1)) obtained from birefringence measurements.

The results of the orientation analysis for the drawn fibres are plotted in *Figure 6*. Similar but less detailed results were obtained more than 30 years ago by Reichle and Prietzsch[11]. *Table 2* and *Table 3* list the detailed results for drawn and heat-set fibres, respectively. Variations in the phase composition, crystalline perfection and other characteristics of the drawn fibres are plotted in *Figures 7* and *8*.

Infra-red spectroscopy

Unpolarized i.r. spectra (1050–850 cm^{-1}) of drawn fibres having high α and γ content and of an amorphous film are shown in *Figure 9*. The high-γ-content fibre was produced by iodination[12]. The pairs of bands at 930, 960 cm^{-1} (α phase) and 919, 977 cm^{-1} (γ phase are associated with the C^{α}–C stretch[12–15]. For each pair of bands, the transition moments are directed parallel and perpendicular to the chain axis, respectively. This is based upon a one-dimensional model for each crystalline phase since the i.r. spectra are not sensitive to the full three-dimensional crystallinity. For determining orientation and composition of the α and γ crystalline phases we

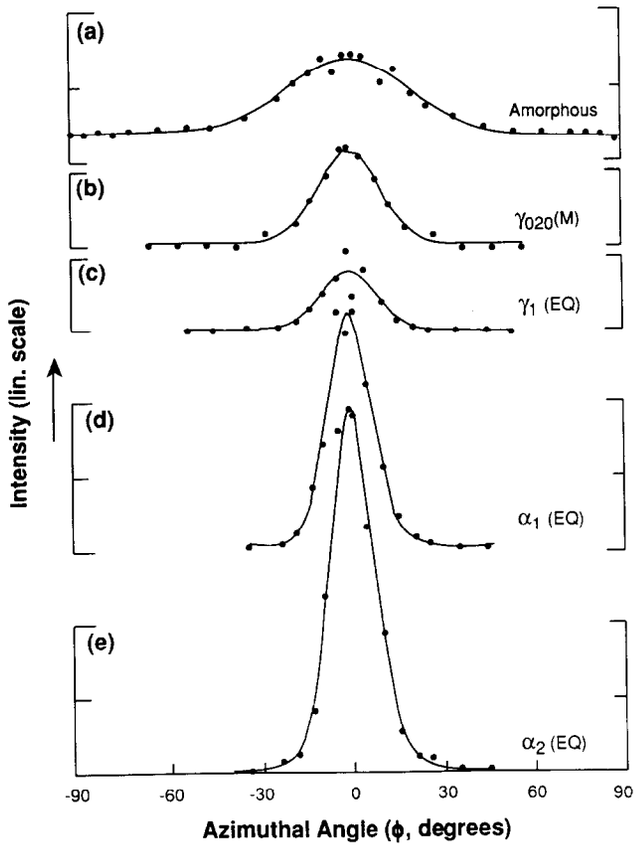

Figure 5 Variations in the crystalline and the amorphous intensities with azimuthal angle: (a) amorphous halo; (b) meridional γ_{020} reflection—this plot is shifted by 90° so that the maximum in this plot overlaps those other equatorial reflections; (c) equatorial γ_1 peak; (d) equatorial α_1 peak; (e) equatorial α_2 reflection

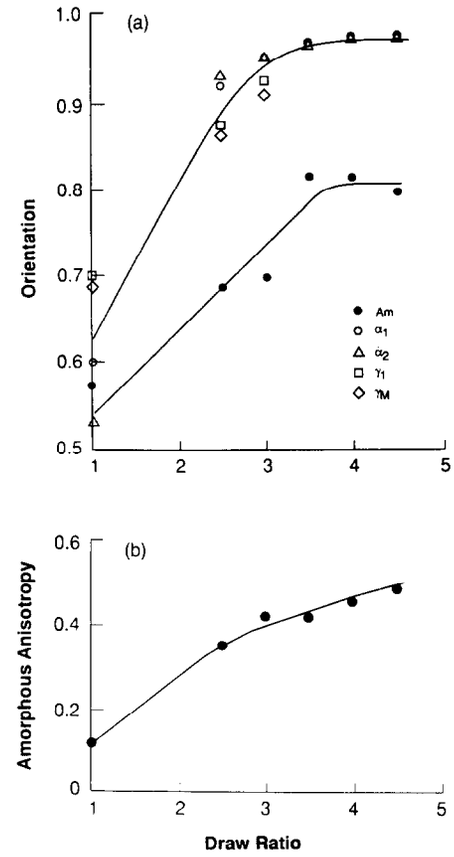

Figure 6 Effect of draw ratio on (a) the degree of orientation of the anisotropic amorphous component and (b) the fraction of the anisotropic amorphous component. The variaion in the crystalline orientation with draw ratio is also shown in the figure

use the 930 and 977 cm^{-1} bands, respectively, and the usual formalism for uniaxial orientation. For the amorphous phase we use the 985 cm^{-1} band whose transition moment direction is unknown.

The effect of processing conditions (e.g. draw ratio) on the polarized i.r. spectra are shown in *Figure 10*. Compositional changes for each phase are more readily observed in *Figure 11*, which shows the corresponding spectra representative of the unoriented sample. These spectra were calculated from the measured polarized spectra assuming uniaxial orientation, according to the formula:

$$A_{\text{unor}} = (A_{\parallel} + 2A_{\perp})/3 \qquad (8)$$

where $A_{\parallel}$ and $A_{\perp}$ are the parallel and perpendicular polarized absorption spectra[13]. *Figure 12* shows typical profile analyses for the undrawn and highly drawn samples in *Figure 10*. In addition to the major bands discussed above it is necessary to include a number of weaker bands due to each of the three phases. Relative changes in composition are obtained from the band areas. The orientation functions for the α and γ phases can be calculated from the polarization ratios of the 930 and 977 cm^{-1} bands, respectively, since the directions of the transition moments are known[16]. This is not the case for the amorphous phase, where we present only the polarization ratios.

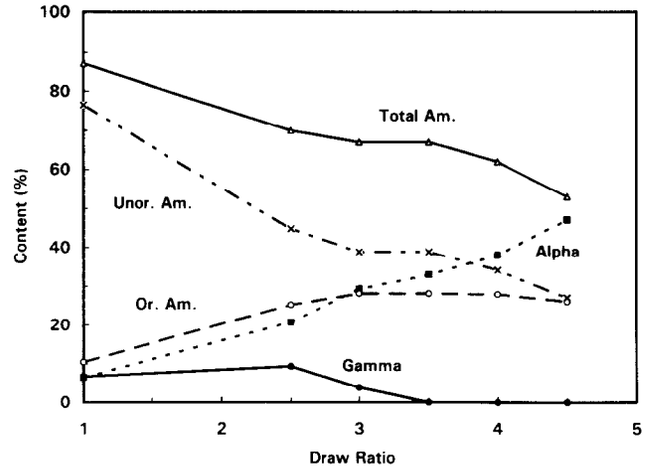

Figure 7 Variations in the phase composition upon drawing. Shown are the α and γ crystallinity, oriented and unoriented amorphous components and the total amorphous content (100 – crystalline index)

From the band areas obtained by profile analyses of the i.r. spectra in *Figure 10* we determined the effect of draw ratio on composition as shown in *Figure 13*. We also determined the dependence of the orientation function for the α and γ phases (*Figure 14a*) and the polarization ratio (of the 985 cm^{-1} amorphous band (*Figure 14b*)) on the draw ratio. The i.r. data indicate that α phase orientation increases dramatically at low DR and reaches a plateau at $DR > 2.5$. Both the γ and the

Table 2 Structural changes in nylon-6 fibres upon drawing

Fibre type, *DR* (Draw ratio)	1.0	2.5	3.0	3.5	4.0	4.5
Density ($g\,cm^{-3}$)	1.1274	1.1343	1.1379	1.1423	1.1445	1.1460
T_g (°C)	10	16	16	19	24	28
Crystalline order						
ICP, 2θ (deg)	2.698	3.067	2.968	3.200	3.156	3.199
ACS (Å) α_1	48	55	58	58	58	62
α_2	33	29	31	34	34	33
γ	71	45				
Composition (%)						
CI	13	30	33	33	38	47
α	6	21	29	33	38	47
γ	7	9	4	0	0	0
AI	87	70	67	67	62	53
unor. amorph.	77	45	39	39	34	27
or. amorph.	10	25	28	28	28	26
Crystalline orientation						
X.r.d. $\Delta\phi(\alpha_1)$ (deg)	57	22.5	17	12.7	12.2	13.8
$f_c(\alpha_1)$	0.596	0.921	0.954	0.974	0.976	0.969
$f_c(\alpha_2)$	0.535	0.941	0.954	0.971	0.972	0.962
$f_c(\gamma_1)$	0.700	0.883	0.924			
$f_c(\gamma_M)$	0.690	0.874	0.903			
Amorphous orientation						
X.r.d. $\Delta\phi$(oa) (deg)	59	48	47	35	36	38
f_{oa}	0.575	0.69	0.7	0.819	0.81	0.791
F_{oa}	0.12	0.36	0.42	0.42	0.45	0.49
f_{ax}	0.039	0.133	0.162	0.155	0.169	0.196
Optical birefr.	0.01499	0.04317	0.04786	0.05160	0.05343	0.05677
f_{ab}	0.1246	0.3354	0.3797	0.4411	0.4237	0.3938

Table 3 Structural changes in nylon-6 fibres upon annealing. NHS = nonheat set; HS = heat set

	Fibre A		Fibre B		Fibre C		Fibre D	
Fibre type Process history	NHS	HS	NHS	HS	NHS	HS	NHS	HS
Density ($g\,cm^{-3}$)	1.1456	1.1545	1.1408	1.1534	1.1408	1.1511	1.1436	1.152
T_g (°C)	39	18	22	9	14	−6	14	−3
Crystalline order								
ICP, 2θ (deg)	3.417	3.961	3.337	3.988	3.275	4.033	3.247	3.922
ACS (Å) α_1	60	93	61	98	66	104	76	103
α_2	32	45	36	51	35	51	39	50
γ			58		54			
Composition (%)								
CI	30	35	29	43	24	42	27	38
α	28	35	20	42	16	42	24	38
γ	2	0	9	1	8	0	3	0
AI	70	65	71	57	76	58	73	62
unor. amorph.	39	44	44	39	49	43	49	45
or. amorph.	31	21	27	18	27	15	24	17
Crystalline orientation								
X.r.d. $\Delta\phi(\alpha_1)$ (deg)	13.5	16.5	21.7	17.4	22.8	20.4	21.4	18
$f_c(\alpha_1)$	0.97	0.956	0.924	0.952	0.918	0.934	0.93	0.948
$f_c(\alpha_2)$	0.963	0.945	0.92	0.946	0.925	0.916	0.93	0.941
$f_c(\gamma_1)$			0.897		0.913			
$f_c(\gamma_M)$			0.904		0.916		0.928	
Amorphous orientation								
X.r.d. $\Delta\phi$(oa) (deg)	37	32	36	34	41	31	32	32
f_{oa}	0.8	0.85	0.81	0.83	0.76	0.85	0.85	0.85
F_{oa}	0.44	0.32	0.38	0.31	0.35	0.26	0.33	0.28
f_{ax}	0.169	0.101	0.134	0.102	0.127	0.078	0.103	0.084
Opical birefr.	0.05720	0.05340	0.05650	0.05790	0.05280	0.06040	0.05930	0.06430
f_{ab}	0.5747	0.469	0.5905	0.4854	0.5847	0.5708	0.649	0.6687

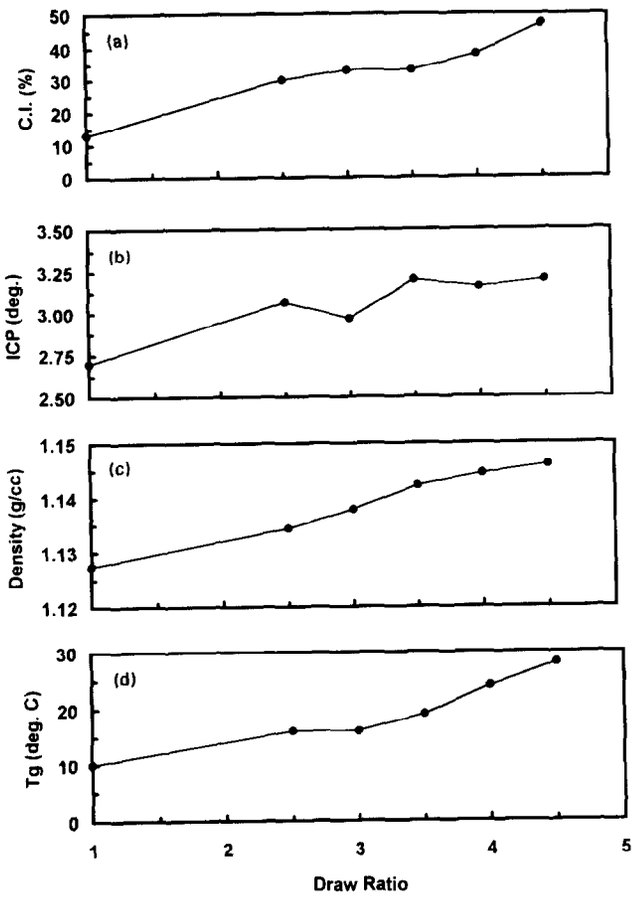

Figure 8 Changes in the crystalline index, index of crystalline perfection, density and T_g with draw ratio

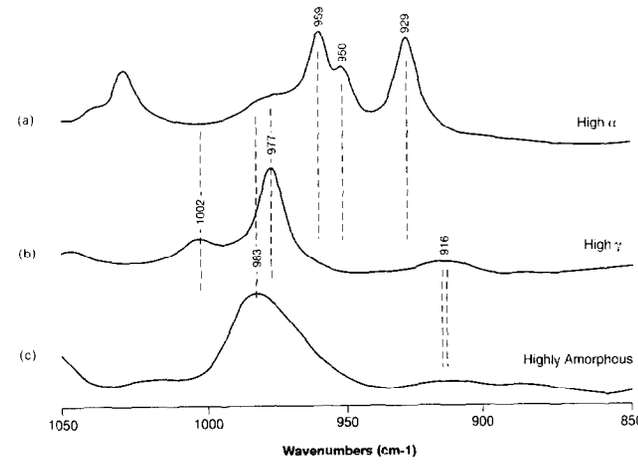

Figure 9 Unpolarized i.r. spectra (1050–850 cm^{-1}) of nylon-6: (a) high-α-content fibre; (b) high-γ-content fibre; (c) highly amorphous, quick-quenched film

amorphous phase show a small degree of orientation in the undrawn fibre. Upon drawing, the orientation of the remaining γ phase increases substantially at low draw ratios. It then appears to decrease, but the γ levels are low, adding significant error to the measurement. Again, the amorphous phase shows a small degree of orientation, which does not appear to change with draw ratios.

Table 4 Structural changes in nylon-6 fibres upon annealing (i.r. results)[a]. NHS = nonheat set; HS = heat set

	Fibre B		Fibre C		Fibre D	
	NHS	HS	NHS	HS	NHS	HS
Composition (%)						
α	27	53	30	52	35	47
γ	57	20	52	24	35	22
amorph.	16	27	18	24	29	31
Orientation ($A_\parallel/A_\perp$)[b]						
α	—	—	10.8	11.8	12.9	14.3
γ	—	—	0.27	0.39	0.68	0.73
amorph	—	—	0.73	0.83	0.82	0.91

[a] The α, γ and amorphous values are calculated assuming i.r. absorption coefficients of each phase are equal, and hence these are not absolute values

[b] Orientation is given as the polarization ratio

Among the four fibres chosen to study the effects of heat setting, two of the yarns (fibres B and C) had substantial γ crystallinity, much higher than for the other two yarns. The primary effect of heat setting is to convert the γ crystalline fraction into α, while the amorphous content remains relatively unchanged, yielding yarns with similar high levels of α crystallinity and low γ crystallinity (*Table 4*). The already high orientation of the α crystalline fraction increases further by a small amount upon heat setting while the amorphous phase, which shows a small degree of orientation, appears to be unchanged (*Table 4*).

Density, birefringence and T_g

The density, optical birefringence values and T_g are listed in *Tables 2* and *3*. The changes in the density with draw ratios are plotted in *Figure 8*, and the density values are plotted against the X.r.d. crystallinities in *Figure 15*. The amorphous orientation f_{ab} calculated using the birefringence values and the X.r.d. crystallinities are tabulated in *Tables 2* and *3*. The T_g increases with draw ratio (*Table 2* and *Figure 8*), and decreases upon heat setting (*Table 3*).

DISCUSSION

In our analysis we have assumed that a semicrystalline polymer such as nylon-6 can be described by a model consisting of crystalline and amorphous phase. The amorphous domains can more accurately be described as non-crystalline, because these domains have some degree of medium-range order, which is not expected in a truly amorphous phase. However, we will continue to use the terms 'amorphous' and 'non-crystalline' interchangeably. Just as the crystalline phase can have varying degrees of order, the amorphous phase can also have varying degrees of disorder. The different crystalline structures (monoclinic and orthorhombic in polyethylene, α and γ in nylon-6, etc.) that are often present in polymers are conventionally regarded as being a part of a single crystalline phase. Similarly, we can regard the amorphous domains with different structural features, the isotropic and the anisotropic domains, as a part of a common non-crystalline phase. Wunderlich and coworkers have recently proposed that the anisotropic amorphous component be identified as a separate phase,

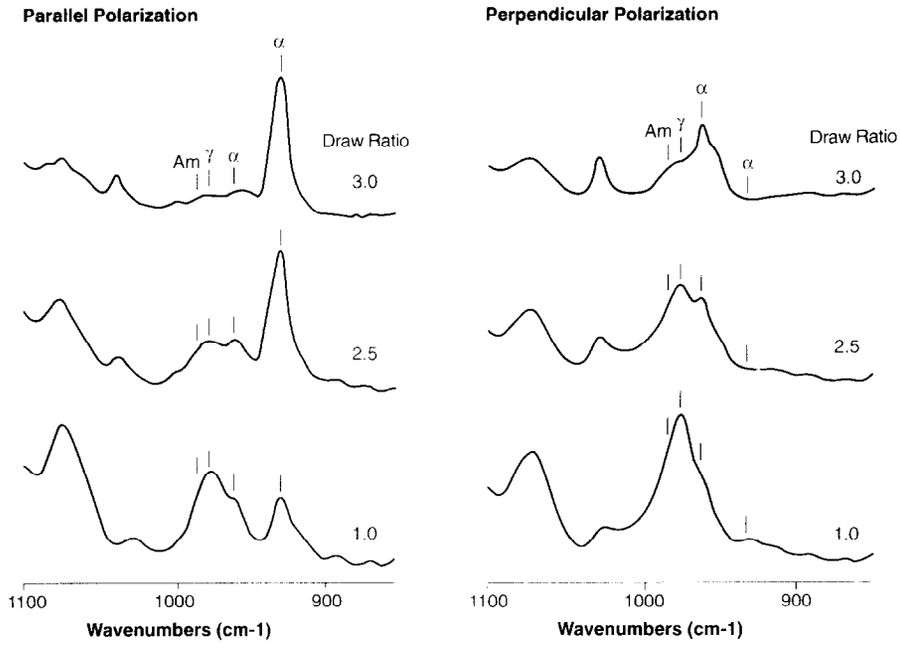

Figure 10 Polarized i.r. spectra of nylon-6 fibres (round cross-section) at various draw ratios for light polarized parallel and perpendicular to the fibre axis

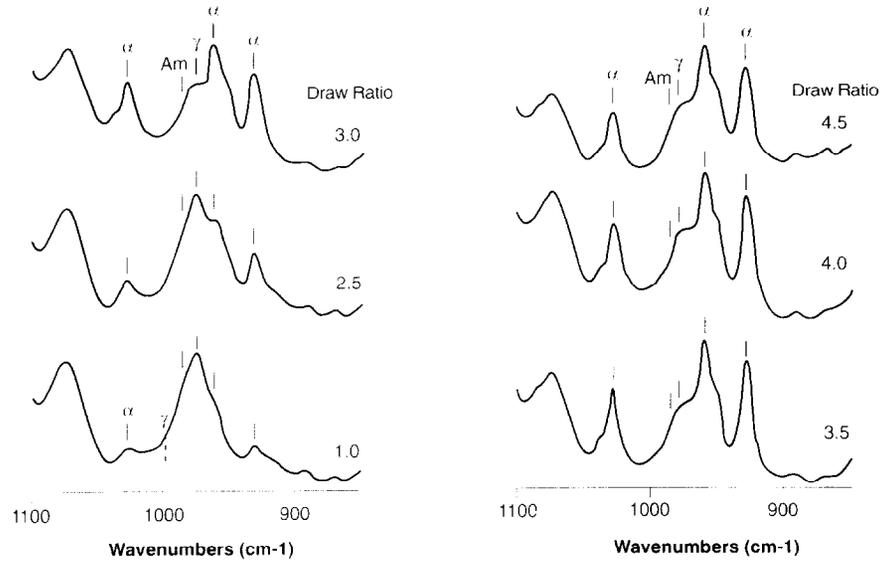

Figure 11 Calculated, unoriented, i.r. spectra of the nylon-6 drawn fibres in *Figure 10*. See text for details

the intermediate phase[17,18]. However, we do not have any compelling evidence to suggest that the anisotropic and isotropic amorphous components are indeed two distinct phases in the same way that the crystalline phase is distinct from the amorphous phase. For instance, solid-state n.m.r does not show two different relaxation behaviours[19]. Furthermore, as will be seen later, the anisotropic component behaves like an 'amorphous' phase in the sense that it exhibits or influences the glass relaxation (*Figure 16*). In contrast, the crystalline phase has little effect on the glass transition behaviour. For these reasons, as well as to maintain continuity with earlier works, we will regard the isotropic and anisotropic 'phases' as two components of the non-crystalline (amorphous) matrix.

In comparing the X.r.d. and i.r. results described here, it is important to note that the size of the segment or the domain being probed by each of these techniques is different. The crystalline parameters derived from wide-angle X.r.d. pertain to domains of 50–100 Å. The amorphous domains observed by X.r.d. have sizes of <20 Å. The i.r. method probes conformations on the scale of ~5 Å in the amorphous phase, and 20 Å (the unit-cell dimension along the chain axis) in the crystalline phase. In both i.r. and X.r.d. methods it is difficult to separate the γ and the amorphous scattering when the γ phase is either poorly formed and/or is very low. The i.r. spectra of the γ and the amorphous phases are very similar to each other, and very different from that of the α phase, suggesting that the γ and the amorphous chains possess very similar conformations. In fact, previous work typically distinguished only two

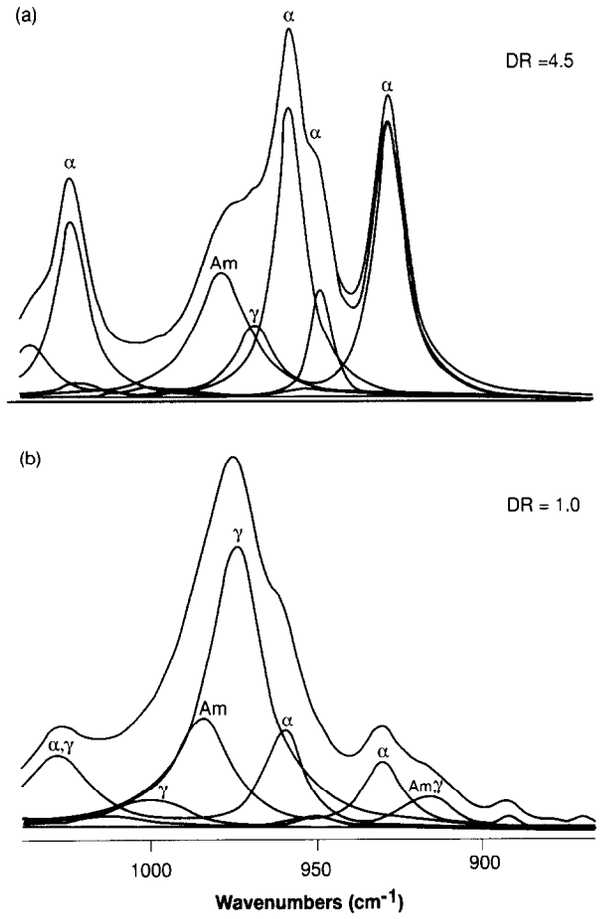

Figure 12 Curve resolution of the i.r. spectra into α, γ and amorphous components for round cross-section nylon-6 fibres having (a) high and (b) low draw ratios

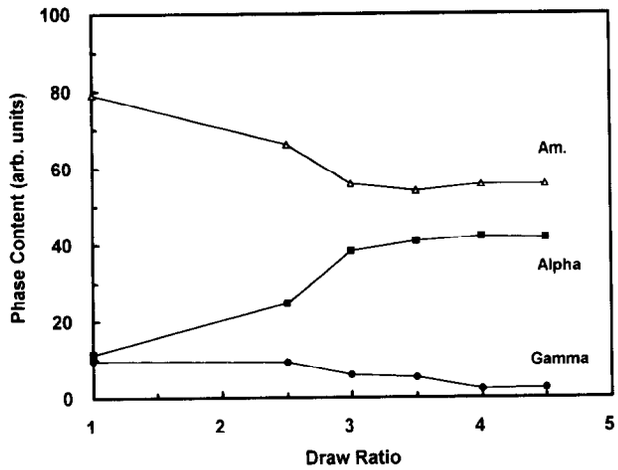

Figure 13 Relative changes in phase composition with draw ratio for round cross-section nylon-6 fibres

conformations, A as in the α phase and B as in the γ phase[13].

The amorphous halo in the X.r.d. pattern of nylon-6 along the equator is narrower than along the meridian (4° compared to 6°), and the position of the amorphous halo depends on the azimuthal angle of the radial scans ($2\theta \sim 21.5°$ near the equator and at $2\theta \sim 20°$ near the meridian). These variations indicate that the amorphous phase is not isotropic. The oriented region is denser than

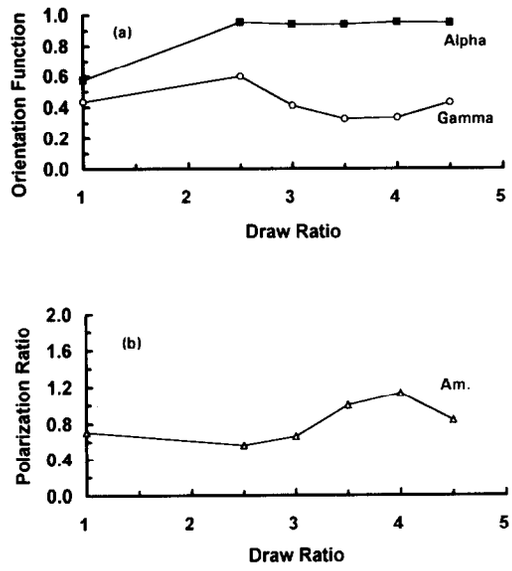

Figure 14 Effect of draw ratio on orientation for round cross-section nylon-6 fibres: (a) orientation function for α and γ phases; (b) polarization ratio of the 983 cm^{-1} band of the amorphous phase

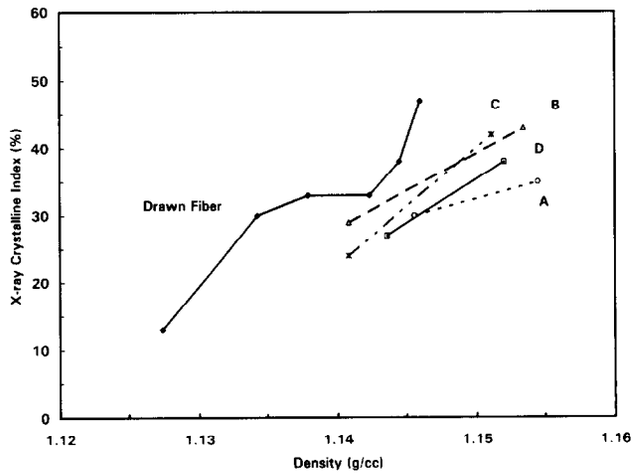

Figure 15 Correlation between crystallinity and density for the various fibres studied in this work. The curves A–D refer to the fibre samples in *Table 3*

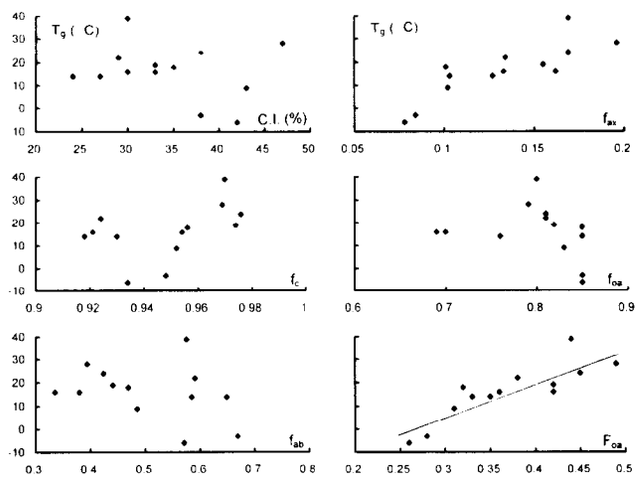

Figure 16 Correlation between T_g and various other structural parameters. *CI* is the crystalline index; f_c is the crystalline orientation; f_{ab} is the amorphous orientation from birefringence data; f_{ax} is the average amorphous orientation from X-ray data; f_{oa} is the degree of orientation of the oriented amorphous component; and F_{oa} is the fraction of the oriented amorphous component

the unoriented region[8]. Thus, as with crystalline density, we expect the average amorphous density to vary with the processing conditions. We also note that the two parameters that describe the amorphous phase, f_{oa} and F_{oa}, do not vary independently of each other. It appears that f_{oa} increases with F_{oa} upon drawing, but decreases with increase in F_{oa} upon annealing. This observation will be discussed later.

The plots of amorphous X.r.d. intensity vs. azimuthal angle (*Figure 5*) show that the amorphous phase is less oriented than the crystalline phase. This is reflected in the degree of orientation of the anisotropic (oriented) amorphous component (f_{oa}). In addition, we also have constant scattering around the azimuth, which appears as a baseline in these azimuthal plots, and which we attribute to isotropic amorphous component. The isotropic and anisotropic domains, if indeed they are physically distinct and not just an artifact convenient for data analysis, are likely to be ~20 Å in size. Unlike the X.r.d. measurements, an average orientation for the amorphous phase is sufficient to explain the i.r. measurements. This fact, together with the differences in the orientation measurement for the two techniques, may arise from the differences in resolving the γ and the amorphous components in the i.r. spectrum. In addition, X.r.d. may not detect γ crystallites <20 Å.

Density is frequently used as a measure of crystallinity. The data in *Figure 15* show that there are two pitfalls in such calculations. First, in many polymers such as nylon-6, there are two crystalline polymorphs, α and γ. The density of γ is lower than that of α (1.17 vs. 1.24 g cm^{-3}). Thus, for the same crystallinity, the density of a γ-rich sample will be lower than that of an α-rich sample. Secondly, the density of the crystalline regions changes with the crystalline perfection. It can be seen from these plots that there are many fibres for which the densities are vastly different although the X-ray crystallinities are about the same. The reason for this discrepancy becomes obvious once we realize that the samples that have higher density also have higher *ICP*. Thus, the higher observed density is not due to higher crystallinity, but to higher crystalline perfection.

Effect of drawing

The most obvious effects of drawing are the increases in crystallinity, crystalline perfection (*ACS* and *ICP*) and orientation (*Table 2*, *Figures 6–8*). Upon drawing, the α crystalline content increases continuously up to the highest draw ratio. The γ crystalline content in the undrawn fibre is low (~8%) and decreases to almost zero at a *DR* of 3.5. The increase in the total crystallinity occurs mostly by the crystallization of the amorphous phase into the α form, which continues up to the highest draw ratio. From the data in *Table 2*, it appears that it is the unoriented amorphous fraction which crystallizes into the α form. On the basis of our earlier small-angle neutron scattering results[20], we speculate that these unoriented domains are in the interlamellar regions. There is also some conversion of the γ phase into the α form. The γ to α conversion ceases at $DR > 3.5$ even though a residual but identifiable fraction of the γ phase remains in the highly drawn fibres.

The crystalline orientation (both α and γ) in X.r.d. increases dramatically at low draw ratios (3–3.5) and remains essentially unchanged at higher draw ratios (*Figure 6a*). The oriented amorphous phase behaves in a similar manner: f_{oa} increases with draw ratio, although it lags behind the crystalline orientation. However, the amorphous anisotropy (F_{oa}, the ratio of the oriented to total amorphous content) continues to increase at $DR > 3$ up to the highest draw ratios studied here (*Figure 6b*). This occurs because the oriented amorphous content is essentially constant at $DR > 3$ whereas the unoriented amorphous fraction continues to decrease and be transformed into α crystals.

Effect of annealing

The most commonly known effects of annealing (heat setting) are the increases in crystallinity and crystalline size. Additionally, there is a large increase in the index of crystalline perfection, which increases the density of the fibre considerably more than that expected by the increase in the crystallinity alone (*Figure 15*). Unlike the effect of drawing, the increase in crystallinity upon heat setting is due to the crystallization of the oriented amorphous fraction (*Table 3*).

The conversion of γ into α upon annealing is almost complete in fibres made at low spin-draw ratios, and there is only a partial conversion of γ into α in fibres made at high spin-draw ratios[21,22]. Our data (*Table 3*) show that the extent of conversion of γ into α is greater in some fibres than in other fibres. The transformation of γ to α is not clearly understood. The currently available evidence suggests that this is a solid-state transformation, although there could be a highly disordered intermediate phase[23]. The stability of the γ phase or the probability that the γ phase is transformed into α depends upon the degree of crystalline perfection of the γ phase, and the presence of the α nuclei[21].

The crystalline orientation normally decreases upon annealing[2]. However, we observe that the crystalline orientation as measured by both X.r.d. and i.r. increases upon heat setting in all fibres except fibre A, which was drawn to a much higher draw ratio (*Table 3*). The increase in crystalline orientation that we observe can be understood if we recall that the increase in crystallinity in these fibres is brought about at the expense of the oriented amorphous chain segments.

Heat setting decreases the average orientation in the amorphous phase. For instance, in X.r.d. there is a consistent decrease in both the average amorphous orientation (f_{ax}) and the anisotropic amorphous fraction (F_{oa}) in all the fibres (*Table 3*). The degree of orientation of the oriented amorphous component (f_{oa}) increases in fibres A, B and C, and remains unchanged in fibre D. I.r. shows a very low degree of amorphous orientation before heat setting and does not change after heat setting. The discrepancy between i.r. and other results is most likely because i.r. is sensitive to local orientation on a molecular scale, whereas X.r.d. measures the orientation of aggregates of polymer chains.

Relation between structure, strength, shrinkage and T_g

The purpose of determining the various structural parameters described here was to be able to predict the properties and performance of the fibre. One of the most obvious differences that stands out in examining the equatorial scans of any nylon-6 fibre is the relative amounts of the α and γ crystallinities. But this α/γ ratio by itself appears to have no significant influence on the

properties of the fibre. The α and γ content is, however, quite useful because it reflects the processing history, and the drawing and annealing conditions of the fibre. The parameters that are likely to be directly useful in predicting the properties are the total crystallinity and the orientation of the fibre. In this section we will attempt to correlate the structural changes to the strength, shrinkage (dimensional stability) and glass transition temperature (T_g) of nylon-6 fibres.

The tensile strength and the modulus of nylon-6 fibres increase substantially after the crystalline parameters, with the exception of total crystallinity, have reached a plateau[3]. It appears that the decrease in the unoriented amorphous component, and the concomitant increase in the α crystallinity, contributes to the higher strength and modulus.

It is tempting to ask if we can predict the shrinkage of a fibre with a knowledge of its structural characteristics. It is generally known that oriented fibres shrink upon annealing. Our data indicate that, upon annealing: (1) crystallinity increases, and (2) the anisotropic amorphous fraction decreases. The extent of unconstrained or free shrinkage upon annealing is the highest in fibre A and least in fibre D (fibre A (23%) > fibre B (16%) ~ fibre C (15%) > fibre D (9%)). This trend is exhibited in both the changes in average amorphous orientation and the anisotropic amorphous fraction in the X.r.d. data. A decrease in the oriented fraction could contribute to shrinkage as the oriented amorphous chain segments crystallize, perhaps epitaxially, onto the existing crystallites. It appears that small apparent crystallite size (*ACS*), a high degree of crystalline perfection (*ICP*) and a large oriented amorphous component lead to most shrinkage.

The value of T_g increases with draw ratio and decreases upon heat setting (*Tables 2* and *3*). The increase of T_g during drawing can be attributed to both the observed increase in the crystallinity and orientation. But note that the T_g decreases upon annealing, which in our fibres also increases their crystallinity. Thus, the increase in crystallinity does not necessarily increase the T_g. This is illustrated in *Figure 16* (or *Tables 2* and *3*), which shows, that T_g is not correlated with parameters that characterize the crystalline regions (crystalline index and crystalline orientation). On the other hand, T_g appears to be influenced by the amorphous orientation. This dependence is seen clearly with the fraction of the oriented amorphous component or F_{oa}, and is much weaker with the average amorphous orientation f_{ax}. One exception to this correlation is the undrawn fibre, which has much higher T_g than can be expected from the correlation shown in *Figure 16* (see *Table 2*; data from the undrawn fibre fall well outside the lower limits of the x values with the exception of *CI*).

One would expect the T_g to increase with the degrees of orientation for the oriented amorphous fraction (f_{oa}). This is true for the drawn series of fibres, but not for the annealed series. The decrease in the fraction of the oriented fractions (F_{oa}) upon annealing appears to have a greater influence on T_g than the increase in f_{oa}. It is possible that the oriented fraction has a T_g distribution whose average value is higher than that of the unoriented fraction. The T_g of the fibre as a whole, being a superposition of these two distributions, would increase with increase in F_{oa}. We came to a similar conclusion in our small-angle neutron scattering studies of hydration in drawn nylon-6 fibres[18]. Thus, T_g is greatly influenced by amorphous anisotropy. The increase in T_g upon drawing is due to an increase in amorphous orientation, and the decrease in T_g upon annealing is due to crystallization of the oriented amorphous chain segments.

ACKNOWLEDGEMENTS

We thank D. Knoop for birefringence measurements, B. Howard and H. Moore for density measurements, and J. Belles for T_g measurements.

REFERENCES

1 Park, J. B., Devries, K. L. and Statton, W. O. *J. Macromol. Sci.–Phys. (B)* 1978, **15**, 229
2 Murthy, N. S., Minor, H. and Latif, R. A. *J. Macromol. Sci.–Phys. (B)* 1987, **26**, 427
3 Gianchandani, J., Spruiell, J. E. and Clark, E. S. *J. Appl. Polym. Sci.* 1982, **27**, 3527
4 Murthy, N. S., Correale, S. T. and Moore, R. A. F. *J. Appl. Polym. Sci., Appl. Polym. Sci. Symp.* 1991, **47**, 185
5 Alexander, L. E. 'X-Ray Diffraction Methods in Polymer Science', Wiley, New York, 1969
6 Samuels, R. J. 'Structured Polymer Properties', Wiley, New York, 1974
7 Murthy, N. S. *Polym. News* 1991, **16**, 358
8 Murthy, N. S., Minor, H., Bednarczyk, C. and Krimm, S. *Macromolecules* 1993, **26**, 1712
9 Balcerzyk, E., Kozlowski, W., Wesolowska, E. and Lewaszkiewicz, W. *J. Polym. Sci., Polym. Phys. Edn.* 1988, **26**, 2573
10 Guinier, A. in 'X-Ray Diffraction', Freeman, San Francisco, 1963, p. 226
11 Reichle, A. and Prietzsch, A. *Angew. Chem.* 1962, **74**, 562
12 Arimoto, H. *J. Polym. Sci. (A)* 1964, **2**, 2283
13 Sibilia, J. P. *J. Polym. Sci. (A2)* 1971, **9**, 27
14 Jakes, J. and Krimm, S. *Spectrochim. Acta (A)* 1971, **27**, 19
15 Jakes, J. and Krimm, S. *Spectrochim. Acta (A)* 1971, **27**, 35
16 Zbinden, R. 'Infrared Spectroscopy of High Polymers', Academic Press, New York, 1964
17 Fu, Y., Busing, W. R., Jin, Y., Affholter, K. A. and Wunderlich, B. *Makromol. Chem.* 1994, **195**, 803
18 Fu, Y., Annis, B., Boller, A., Jin, Y. and Wunderlich, B. *J. Polym. Sci., Polym. Phys.* 1995, **32**, 2289
19 Curran, S.A., unpublished, 1990
20 Murthy, N. S. and Orts, W. J. *J. Polym. Sci., Polym. Phys.* 1994, **32**, 2695
21 Murthy, N. S., Aharoni, S. M. and Szollosi, A. B. *J. Polym. Sci., Polym. Phys. Edn.* 1985, **23**, 2549
22 Salem, D. R., Moore, R. A. F. and Weigmann, H.-D. *J. Polym. Sci., Polym. Phys. Edn.* 1987, **25**, 567
23 Murthy, N. S. *Polym. Commun.* 1991, **32**, 301